

The cell adaptation time sets a minimum length scale for patterned substrates

Diogo E. P. Pinto,^{1,2} Gonca Erdemci-Tandogan,^{3,4} M. Lisa Manning,³ and Nuno A. M. Araújo^{1,2}

¹*Departamento de Física, Faculdade de Ciências,*

Universidade de Lisboa, Campo Grande, P-1749-016 Lisboa, Portugal

²*Centro de Física Teórica e Computacional, Campo Grande, P-1749-016 Lisboa, Portugal*

³*Department of Physics, Syracuse University, Syracuse, New York 13244, USA*

⁴*Institute of Biomaterials and Biomedical Engineering,
University of Toronto, Toronto, ON, M5S 3G9, Canada*

The structure and dynamics of tissue cultures depend strongly on the physical and chemical properties of the underlying substrate. Inspired by previous advances in the context of inorganic materials, the use of patterned culture surfaces has been proposed as an effective way to induce space-dependent properties in cell tissues. However, cells move and diffuse and the transduction of external stimuli to biological signals is not instantaneous. Here, we show that the fidelity of patterns depends on the relation between the diffusion (τ_D) and adaptation (τ) times. Numerical results for the self-propelled Voronoi model reveal that the fidelity decreases with τ/τ_D , a result that is reproduced by a continuum reaction-diffusion model. We derive a minimum length scale for the patterns that depends on τ/τ_D and can be much larger than the cell size.

INTRODUCTION

The regulated growth and maintenance of a living tissue under controlled conditions is a major challenge for cell biology and tissue engineering. The standard procedure consists in the use of culture surfaces to support and guide the cells [1–5]. An extensive body of research shows that the cell morphology and dynamics are sensitive to the physical and chemical properties of the substrate [1, 4, 6–12]. For example, it has been shown that substrate stiffness can significantly affect the geometry of cultured cells, including their spreading area [12, 13], volume [14], and shape elongation [15]. In addition, the nanotopography of the substrate can alter cell polarization, shape, and motility [16–19]. Thus, the effort has been in the design of biocompatible substrates that regulate the individual and collective dynamics of cells.

There is a sustained interest in the possibility of generating spatial patterns of cells with different properties, which is critical for morphogenesis, collective cell motion, and wound healing [16–24]. In development, the processes that typically generate two tissue types separated by a boundary have been studied extensively [25–29], and often occur because two different cell types, through various mechanisms, prefer to be surrounded by cells of the same type [30–34]. However, in vitro, an alternative approach is to culture a single cell type on a patterned substrate, and allow the patterned substrate to change the properties of cells to generate a pattern [16, 18, 19, 21].

Patterned substrates have been used to a large extent in the context of inorganic materials [35–38]. However, their use for biological systems raises several additional difficulties. Besides the need for biocompatible materials, the transduction of external stimuli into biological signals that control the cell morphology and mechanics is not instantaneous. It requires a hierarchy of biochemical processes, which sets a characteristic adaptation time that

can extend over hours [39]. The problem is that, within the adaptation time scale, cells might move around and explore other regions of the substrate. Thus, the fidelity of patterns in the regulation of cell tissues should depend on how the adaptation time compares with the other relevant time scales. This is precisely what we study here.

We consider an epithelial confluent tissue on a simple patterned substrate, consisting of two halves that solely differ in the cell-substrate interaction (see Fig. 1). We describe the tissue with the self-propelled Voronoi model, where the cell-substrate interaction is included in the preferential geometry of each cell, as cell shapes change as a function of substrate properties [13], and cell shape in turn governs the rate of cell diffusion in monolayers [5]. We show that the fidelity of the pattern in the regulation of the tissue properties is compromised significantly when the adaptation time competes with the diffusion time of cells.

MODEL

We model the confluent tissue as a monolayer of N cells using the self-propelled Voronoi model [40–42]. Each cell i is represented by its center \mathbf{r}_i and its shape is given by the Voronoi tessellation of the space. The stochastic trajectories of cells are obtained from a set of Langevin equations of motion,

$$\frac{d\mathbf{r}_i}{dt} = \mu \mathbf{F}_i + v_0 \hat{\mathbf{n}}_i, \quad (1)$$

where \mathbf{F}_i is the net force acting on cell i , μ is the mobility of the cell, v_0 the self-propulsion speed, and $\hat{\mathbf{n}}_i = (\cos\theta_i, \sin\theta_i)$ is a polarity vector which sets the direction of the self-propulsion force. For simplicity, we consider that θ_i is a Brownian process given by,

$$\dot{\theta}_i = \eta_i(t), \quad \langle \eta_i(t) \eta_j(t') \rangle = 2D_r \delta(t - t') \delta_{ij}, \quad (2)$$

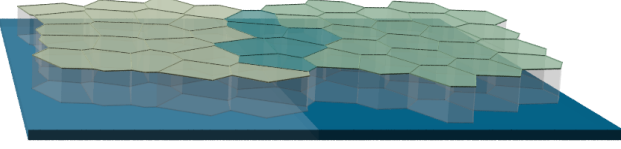


FIG. 1. Schematic representation of the system. We consider a confluent tissue on a squared substrate with two regions of equal linear length $L/2$, which differ in the target value of the shape index p_0 of cells: $p_0 = p_A$ on the brighter side (left) of the substrate and $p_0 = p_B$ on the darker one (right), with $p_B > p_A$. The color of the cells is related to their actual shape index $p_0(t)$, which is equal to p_A for the ones in the left and p_B for the ones in the right. The darker cells (in the middle) have an intermediate value of $p_0(t)$, i.e., $p_A < p_0(t) < p_B$.

where $\eta_i(t)$ is an uncorrelated random process of zero mean and its variance sets the rotational diffusion D_r .

The net force \mathbf{F}_i describes the multibody cell-cell interaction and it is given by $\mathbf{F}_i = -\nabla E_i$, where E_i is the energy functional for cell i [43, 44],

$$E_i = K_A[A_i - A_0]^2 + K_P[P_i - P_0]^2, \quad (3)$$

where A_i and P_i are the area and perimeter of cell i , respectively, and A_0 and P_0 are their target values. The first term accounts for the cell incompressibility and the resistance to height fluctuations. The second term accounts for the active contractility of the actomyosin subcellular cortex and effective cell membrane tension, due to cell-cell adhesion and cortical tension. K_A and K_P are the area and perimeter moduli. By rescaling energy in units of $K_A A_0^2$, we obtain four adimensional quantities: two that characterize the area and the perimeter of the cell ($a_i = A_i/A_0$ and $p_i = P_i/\sqrt{A_0}$), a shape parameter $p_0 = P_0/\sqrt{A_0}$, and $r = K_A A_0/K_P$ (see *Supplementary Information*). Without loss of generality, below, all lengths are in units of $\sqrt{A_0}$ and time is in units of $1/(\mu K_A A_0)$.

Cells diffuse with a diffusion coefficient D that depends on the four control parameters: the speed of self-propulsion v_0 , the rotational diffusion D_r , the shape index p_0 , and the ratio r . For fixed values of v_0 and D_r , as considered here, the model yields a rigidity transition at a threshold value of the shape index $p_0 = p_c$: from a solid-like state with finite shear modulus, for $p_0 < p_c$, to a fluid-like state of zero rigidity, for $p_0 > p_c$, where cell rearrangements are more frequent [40, 45].

We consider a squared substrate of linear length $L = \sqrt{N}$, where the value of the target shape index (p_0) is spatially dependent. As schematized in Fig. 1, we split the substrate in half, with different values of p_0 in each side. Thus, cells on the left-hand side have a target $p_0 = p_A$, while the ones on the right-hand side have $p_0 = p_B$, where $p_B > p_A$. When a cell diffuses from one side to the other, their target value of the shape index in Eq. (3)

changes accordingly, within a characteristic adaptation time τ . Thus, we consider that the time dependence of the shape index $p_{0,i}$ for cell i is given by,

$$\dot{p}_{0,i}(\Delta t_i) = \frac{1}{\tau}[p_{0,i}(\infty) - p_{0,i}(\Delta t_i)], \quad (4)$$

where Δt_i is the time interval since the cell crossed the line dividing the substrate, for the last time. $p_{0,i}(0)$ is the shape index of cell i before crossing and $p_{0,i}(\infty)$ is the target value in the new side.

RESULTS

To study the role of the adaptation time τ , we first consider a pair of values for the shape index for which the confluent tissue is in a fluid-like state at both sides of the substrate: $p_A = 3.875$ and $p_B = 3.9$. For these values, the cell diffusion coefficients on each side differ by less than 15%: $D_A = 3.61 \times 10^{-3}$ and $D_B = 4.13 \times 10^{-3}$, obtained from the mean squared displacement. Below, we assume $D_A = D_B = D$.

Initially, all cells are fully adapted to the underlying substrate (see *Methods*). As time evolves, cells diffuse and cross from one side to the other. However, due to the finite adaptation time, their target shape index $p_{0,i}$ changes in time, as given by Eq. (4), and thus cells of different shape indices mix in both sides of the substrate. To characterize this mixing, we measure the demixing parameter, D_p , defined as,

$$D_p = \frac{1}{N} \sum_i \frac{1}{N_{i,neigh}} \sum_j^{N_{i,neigh}} H(\epsilon - |p_{0,i} - p_{0,j}|), \quad (5)$$

where the out sum is over all cells and the inner sum is over the $N_{i,neigh}$ neighbors of cell i [34]. $H(\epsilon - |p_{0,i} - p_{0,j}|)$ is the Heaviside step function and ϵ is a threshold that we set to $\epsilon = 10^{-5}$ (see *Supplementary Information* for the dependence on ϵ). For $D_p = 1$ the cells in the confluent tissue are completely segregated by their shape index, whereas for $D_p = 0$ they are fully mixed, i.e., each cell is surrounded by cells with a different shape index.

Figure 2(a) shows the time dependence of the demixing parameter for different values of the adaptation time τ , where time is rescaled by τ . As cells mix, D_p decreases and saturates asymptotically. Different curves are for different values of τ/τ_D , where $\tau_D = L^2/D$ is the diffusion time. In Fig. 2(b) is the asymptotic value of D_p as a function of τ/τ_D for different numbers of cells (same density). A data collapse is observed, which shows that finite-size effects are negligible. The monotonic decrease of the asymptotic value of D_p with τ/τ_D hints at a competition between two time scales: the adaptation and the diffusion time. When the adaptation time is negligible ($\tau \ll \tau_D$), cells adapt rapidly to the underlying substrate, with $D_p \approx 1$. When the two time scales

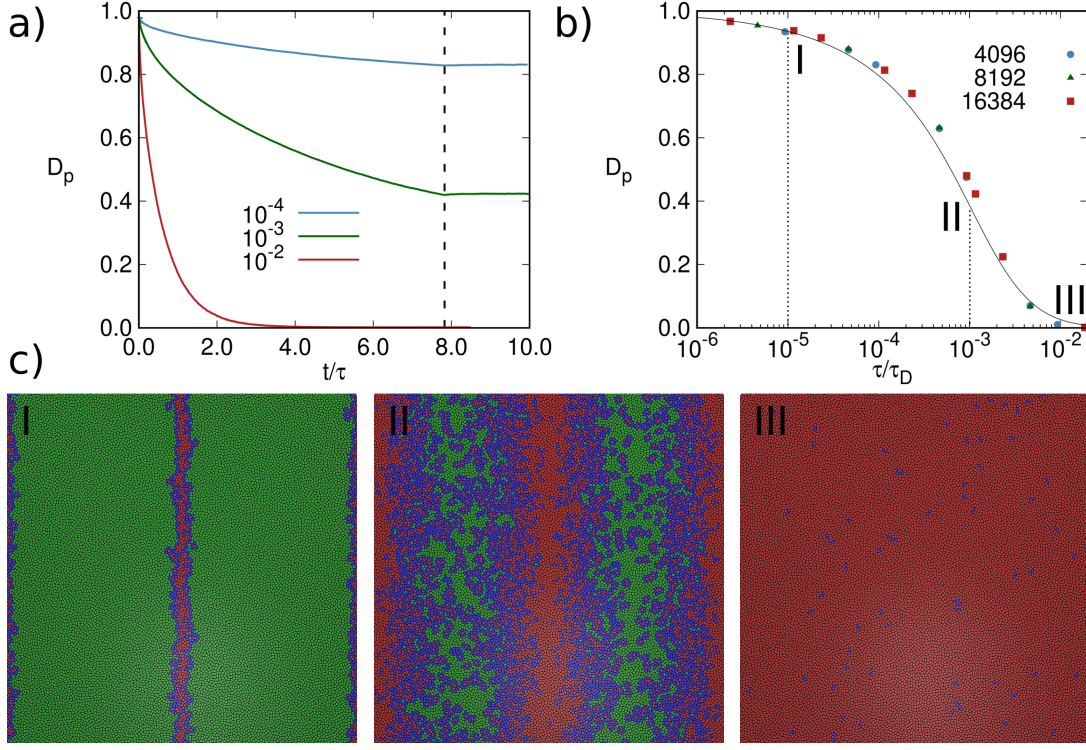


FIG. 2. Dependence of the demixing parameter D_p on the two relevant time scales: adaptation τ and diffusion τ_D times. (a) Time dependence of the demixing parameter, where time is rescaled by the adaptation time τ . Different curves are for different values of τ/τ_D , namely, 10^{-4} , 10^{-3} , and 10^{-2} . The vertical dashed line corresponds to $\ln[(p_B - p_A)/\epsilon]$, which is the time it takes for the target shape index of a cell i that crosses to the right-hand side, with $p_{0,i} = p_B$ to become $p_{0,i} = p_A + \epsilon$, as given by Eq. (4). (b) Demixing parameter as a function of τ/τ_D for different system sizes, where the number density of cells is kept constant to unity, i.e., $L = \sqrt{N}$. The (black)-solid line is given by Eq. (8), derived from a continuum model, with $\alpha = 0.0866 \pm 0.0009$. (c) Snapshots of the confluent tissue obtained numerically at time 10τ , for three different values of τ/τ_D , namely, 10^{-5} , 10^{-3} , and 10^{-2} . The color of each cell depends on the demixing parameter: green ($D_p = 1$), red ($D_p = 0$), and blue ($0 < D_p < 1$). It is clear that the cluster of red cells is formed around the line dividing the substrate into two parts (see Fig. 1) and it grows with τ/τ_D until it spans the entire tissue. Results in (a) and (b) are averages over ten independent samples.

compete, the value of D_p should depend on the ratio between the two. In the limit where they are of the same order, D_p should vanish, for the cell changes sides before fully adapting to the new shape index. Thus, large values of the adaptation time compromise the control over the shape of the tissue boundaries via patterned substrates.

The demixing parameter is not uniformly distributed in space. In Fig. 2(c) are three snapshots of the tissue obtained at time 10τ , for different values of τ/τ_D . The color of cells depends on the value of the demixing parameter. Cells that are surrounded by cells of the same target shape index p_0 are in green ($D_p = 1$), the ones surrounded by cells of a different p_0 are in red ($D_p = 0$). The ones with intermediate values of D_p are in blue. One clearly sees that the green cells are in the center of each half, whereas red cells are concentrated around the boundaries: middle and borders, due to the periodic boundary conditions. However, the width of the regions of green and red cells depends on the value of τ/τ_D .

We define $u(x, t)$ as the fraction of cells that are green

($D_p = 1$) at time t , where $x \in [0, L]$ is the spatial coordinate along the horizontal direction. To compute $u(x, t)$ numerically, we divide the system into vertical slices and measure the fraction of cells with $D_p = 1$ within each slice. The results for $u(x, 10\tau)$, for different values of τ/τ_D are shown in Fig. 3(a), for $x \in [0, L/2]$. As suggested by Fig. 2(c), there are more green cells at $x = L/4$ but, the fraction of cells and the width of the profile decreases with τ/τ_D . The latter scales with $\sqrt{\tau/\tau_D}$ as expected for a diffusive process (see Fig. 3(b)).

To describe the competition between cell diffusion and adaptation time, we now propose a continuum model to describe the time evolution of $u(x, t)$. For simplicity, we take advantage of the symmetry of the problem and only focus on $x \in [0, L/2]$. We consider a reaction-diffusion equation for $u(x, t)$,

$$u_t(x, t) = D^* u_{xx}(x, t) + T[1 - u(x, t)]. \quad (6)$$

where u_t is the time derivative and u_{xx} is the second space derivative. The first term on the right-hand side is

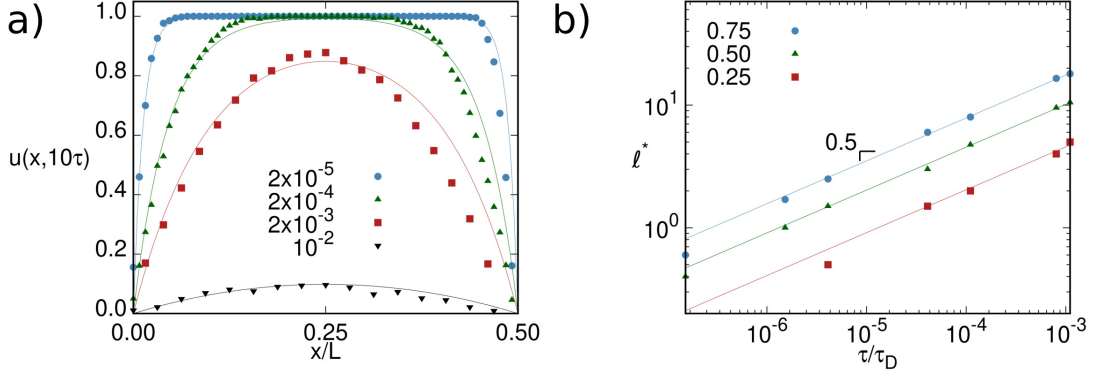


FIG. 3. Spatial distribution of cells with $D_p = 1$. (a) Profile $u(x, t)$ of the fraction of cells with $D_p = 1$, for different values of τ/τ_D , where x is the spatial coordinate along the horizontal direction, $t = 10\tau$, τ is the adaptation time, and τ_D the diffusion time. The lines are given by Eq. (7), which is derived from a continuum model, using ϕ as a fitting parameter. (b) Value of $x = \ell^*$ at which $u(\ell^*, 10\tau)$ is 0.25 (squares), 0.50 (triangles) or 0.75 (circles), as a function of τ/τ_D . Results are averages over ten independent samples.

a diffusive term that describes the collective diffusion of cells, with an effective diffusion coefficient D^* . The second term is a reaction term, which describes the adaptation of cells to the local environment. The adaptation is proportional to the fraction of cells that are not adapted, i.e. $1 - u(x, t)$, and occurs at a rate T that is proportional to the inverse of the adaptation time τ . Since we start from a demixed state, the initial conditions are $u(x, 0) = 1$ and the boundary conditions are $u(0, t) = u(L/2, t) = 0$ at all times.

As derived in the *Supplementary Information*, the control parameter for the dynamics of the continuum model is the ratio $\phi^2 = T(L/2)^2/D^*$. Since $T \sim \tau^{-1}$ and $D^* \sim D$, then $\phi^2 \sim L^2/\tau D = \tau_D/\tau$, which is the ratio between the diffusion and adaptation time scales. We define $\phi^2 = \alpha L^2/\tau D$, where α is a prefactor that depends on the geometry of the substrate and the value of the shape index on both sides. Asymptotically, $u(x, t)$ converges to a stationary state $u_E(\hat{x})$,

$$u_E(\hat{x}) = \frac{1 + e^\phi - e^{-\phi(\hat{x}-1)} - e^{\phi\hat{x}}}{1 + e^\phi}, \quad (7)$$

where $\hat{x} = 2x/L$. As shown in Fig. 3(a), this analytical solution (solid lines) is in qualitative and quantitative agreement with the numerical results for the self-propelled Voronoi model, where we set $\alpha = 0.0866 \pm 0.0009$ for all curves, obtained by a fit using the least squares method.

To compute the demixing parameter from the profile in the stationary state, $u_E(x)$, we consider a mean-field approach, where the probability that two neighboring cells are in the same state is $u_E^2(x)$ and so $D_p = \int_0^1 u_E^2(\hat{x}) d\hat{x}$, which gives,

$$D_p = 1 + \frac{1}{1 + \cosh(\phi)} - \frac{3 \tanh(\phi/2)}{\phi}. \quad (8)$$

This solution is the solid line in Fig. 2(b), which is in quantitative agreement with the numerical results.

The numerical and analytical results suggest that the fidelity of a patterned substrate in the control of the morphology of a tissue is significantly dependent on the ratio between the diffusion and the adaptation time. Ideally, full control would imply $D_p = 1$. The lower is the value of D_p , the less efficient is the use of a pattern. Let us define δ such that a tissue with $D_p < \delta$ is considered mixed. Since D_p increases monotonically with ϕ (see Fig. 2(b)), we take the limit of vanishing ϕ and D_p . From a Taylor expansion about $\phi = 0$, we obtain $D_p = \phi^4/120 + O(\phi^5)$. Thus, there is a minimum length,

$$L_{\min} = \left[\frac{\tau D}{\alpha} \sqrt{120\delta} \right]^{\frac{1}{2}}, \quad (9)$$

below which the cells in the tissue are mixed, which sets a lower bound for the size of the patterns.

So far, we considered a pair of target shape indices such that both sides are in a fluid-like state. We study now the solid-fluid case, by setting $p_A = 3.65 < p_c$ and $p_B = 3.9$ (as before). Figure 4(a) shows the time dependence of the demixing parameter for the side A , B , and both sides. Different from the fluid-fluid case, where the time dependence of D_p was similar for both sides, here we observe that D_p vanishes for the liquid-like side, whereas in the solid-like side it saturates at ≈ 0.8 . This break of symmetry is observed for a wide range of parameters, as seen in Fig. 4(b) from the dependence of the value of D_p on the left- and right-hand sides on τ/τ_D , where τ_D is the one for the liquid-like state. For all values of τ/τ_D the demixing parameter is higher in the solid-like state than in the liquid one. This asymmetry stems from the difference in the effective value of the diffusion coefficient D in both sides. For the solid-like state, $D \approx 0$ and thus adaptation is much faster than diffusion. Cells have

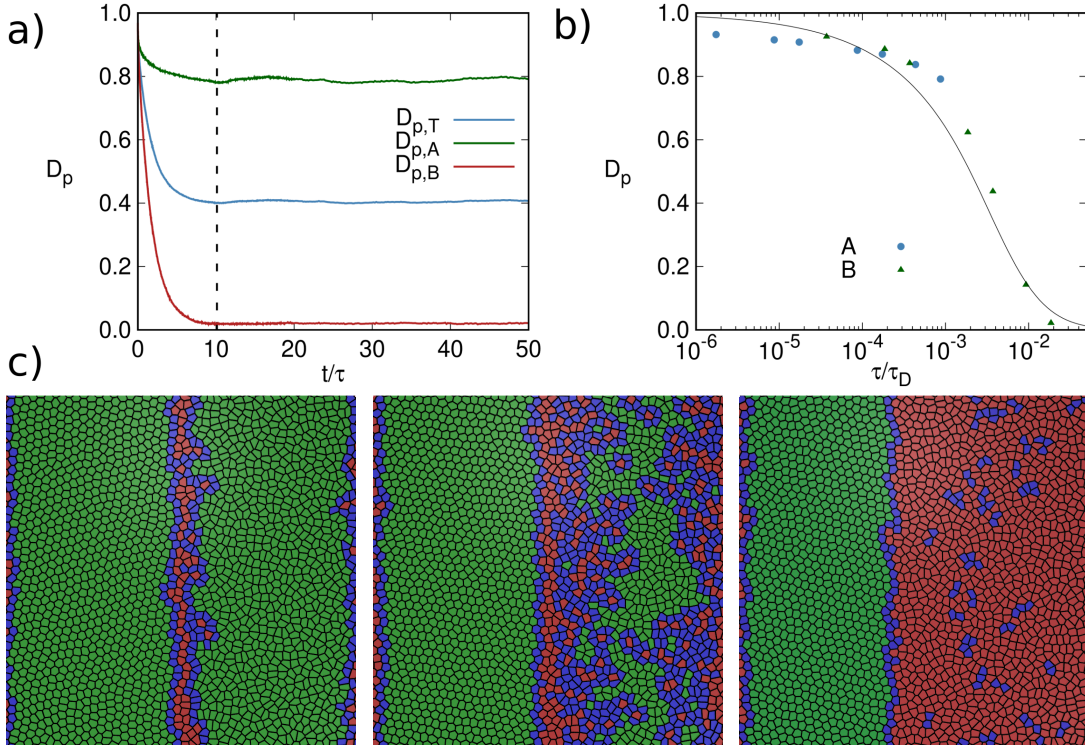


FIG. 4. Dependence of the demixing parameter for the solid-fluid case. (a) Time dependence of the demixing parameter, where time is rescaled by the adaptation time ($\tau = 5000$), for $N = 2048$. Different curves are for the side A, B, and both sides. (b) Demixing parameter as a function of τ/τ_D for both sides, obtained at 50τ . The (black)-solid line is given by Eq. (8), derived from the continuum model, with $\alpha = 0.276 \pm 0.003$. (c) Snapshots of the confluent tissue, obtained numerically for different values of τ/τ_D , namely, 10^{-3} , 10^{-2} , and 10^{-1} . The color of each cell depends on the demixing parameter: green ($D_p = 1$), red ($D_p = 0$), and blue ($0 < D_p < 1$). Results in (a) and (b) are averages over ten independent samples and the value of τ_D is obtained for the liquid-like side.

enough time to adapt to the new target shape index, which yields a high value of D_p that does not depend strongly on τ (see also snapshot for different values of τ in Fig. 2(c)). By contrast, for the liquid-like state, the value of D_p strongly depends on the value of τ as in the liquid-liquid case, see Fig. 2. In fact, the dependence of D_p on τ/τ_D in Fig. 4 for the liquid-like side is well described by Eq. (8), solid curve in Fig. 4(b) (further results for different substrates are discussed in the *Supplementary Information*).

CONCLUSION

We included the adaptation time of cells to external stimuli in a minimal model for confluent tissues. We found that the use of patterned substrates to regulate the tissue properties is compromised significantly when the adaptation time competes with the cell diffusion time. The latter depends on the characteristic length of the pattern L^* . From a continuum description based on a reaction-diffusion equation, we derived an analytic expression for the minimum length L_{\min} for the pattern to be effective. For $L^* > L_{\min}$, cells have enough time

to adapt to the local cell-substrate interaction and the heterogeneous distribution of cell shapes reproduces the symmetries of the pattern, with a clear segregation by shape index. By contrast, for $L^* < L_{\min}$, cells do not fully adapt to the local cell-substrate interaction and their shape index depends on their individual trajectories.

For inorganic materials, the goal has been to reduce the length scale of the patterns and achieve a control at the level of an individual particle [38, 46]. By contrast, in the case of cell tissues, we show that the relevant length scale is set by the dynamics. Experimentally, it was shown that cells cultured on a shape memory polymer substrate take about 36 hours to adapt to changes in the structure of the substrate [47]. If we consider a typical diffusion coefficient of a cell in a confluent tissue of $D \approx 0.1 \mu\text{m}^2 \text{min}^{-1}$ [5], from Eq. (9), we obtain that $L_{\min} \approx 55 \mu\text{m}$, which is roughly four times the size of a single cell.

We considered a simple pattern but, it is straightforward to extend the conclusions to other patterns. In fact, the competition between diffusion and adaptation is so general that it should apply even to heterogeneous

random substrates. These substrates are usually characterized by a correlation length ξ that plays the role of L^* . So, only for $\xi > L_{\min}$, cells are expected to segregate based on their shape index, as defined by the local properties of the substrate.

The identification of the mechanisms responsible for the emergence of spatial cell patterns in a developing organism has been a subject of intensive research and discussion over the years [25, 30, 32, 48]. A recent study combines theory and experiments to show that cell sorting and compartmentalization in living organisms might be driven by surface tension due to differential adhesion [34]. However, the use of cell mixtures in vitro encompasses multiple challenges, which include the lack of control over the spatial distribution of cell types. We have shown that, above a certain length scale, the spatial distribution of cell properties can be controlled by the substrate pattern.

For simplicity, we assumed that the cell-cell and cell-substrate interactions depend on the substrate but not on the cell itself. A recent study shows that a broad distribution of the shape index of cells affects the tissue rigidity and, consequently, the cell diffusion coefficient [49]. Understanding the role of cell heterogeneities in the adaptation time is a question of interest for future studies.

METHODS

To simulate the confluent tissue, we used a recently developed hybrid CPU/GPU software package, cell-GPU [50], for the self-propelled Voronoi model. The equations of motion (1) are integrated using the Euler method, with a time step of $\Delta t = 10^{-3}$. We impose periodic boundary conditions, $D_r = 1$, $v_0 = 0.3$, and $r = 100$, the latter to guarantee that fluctuations in the cell area are negligible when compared to the ones in the perimeter. For the considered set of parameters, the rigidity transition occurs for $p_c \approx 3.725$ [40]. To generate the initial configuration, we generate N positions at random and let the system relax over 10^4 time steps, with $p_0 = p_B$ for all cells. Then, we set $p_{0,i}(0) = p_A$ for the cells in the left- and $p_{0,i}(0) = p_B$ for the ones in the right-hand side of the substrate.

ACKNOWLEDGMENTS

The authors acknowledge financial support from the Portuguese Foundation for Science and Technology (FCT) under Contracts no. PTDC/FIS-MAC/28146/2017 (LISBOA-01-0145-FEDER-028146), UIDB/00618/2020, UIDP/00618/2020 and SFRH/BD/131158/2017. MLM and GET acknowledge

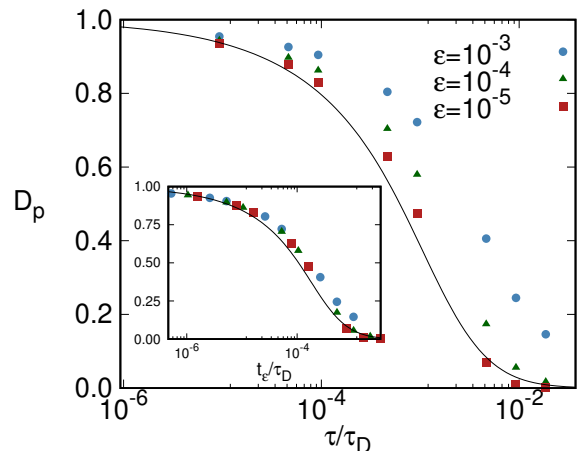


FIG. 5. Asymptotic demixing parameter D_p as a function of τ/τ_D , for $N = 4096$. Different curves are for different values of ϵ , namely, 10^{-5} , 10^{-4} , and 10^{-3} . All the other parameters are the same as in the fluid-fluid case of the main paper. In the inset, a data collapse is obtained when time is rescaled as proposed in Eq. (11). Results are averages over ten independent samples.

support from the Simons Foundation (#446222) and from NSF-DMR-1352184 (MLM).

SUPPLEMENTARY INFORMATION

Reduced units

If we rescale energy in units of $K_A A_0^2$, the energy functional E_i given by Eq. (3) is,

$$e_i = (a_i - 1)^2 + \frac{(p_i - p_0)^2}{r}, \quad (10)$$

where $e_i = E_i/K_A A_0^2$, $a_i = A_i/A_0$ and $p_i = P_i/\sqrt{A_0}$ are the area and perimeter of cell i in adimensional units, $p_0 = P_0/\sqrt{A_0}$ is the shape index, and the ratio $r = K_A A_0/K_p$ sets the ratio between the area and the perimeter moduli.

Influence of ϵ on the results

In Eq. (2), the definition of alike cells depends on a threshold ϵ , which we fixed at $\epsilon = 10^{-5}$. In practice, the value of these ϵ will depend on the experimental resolution to segregate cells by their type. Here, we study the dependence on ϵ .

Figure 5 shows the time dependence of the demixing parameter D_p for different values of ϵ for the fluid-fluid case as in the main paper. The larger is the value of ϵ , the more cells are considered to be alike and therefore, the value of D_p is larger. To compare results for different

values of ϵ , we compute the time t_ϵ that takes for a cell to adapt to a new target shape index, within a threshold ϵ . If the time evolution of the shape index is given by Eq. (4),

$$t_\epsilon = \int_\epsilon^{\Delta p_0} -\tau \ln\left(\frac{\epsilon}{\delta_p}\right) d\delta_p, \quad (11)$$

where $\Delta p_0 = p_B - p_A$ is the change in shape index. In the inset of Fig. 5 we show that a data collapse is obtained for a wide range of values of ϵ (three orders of magnitude), if we plot D_p as a function of t_ϵ .

Time dependent solution for the continuum model

To solve Eq. (6), we define a characteristic length $L^* = L/2$ and time $T^* = L^2/4D^*$, respectively, and introduce two adimensional variables,

$$\hat{x} = \frac{2x}{L} \quad \hat{t} = \frac{4D^*t}{L^2}. \quad (12)$$

Using the chain rule, we get the following identities,

$$u_t = \frac{1}{T^*} u_{\hat{t}} \quad \text{and} \quad u_{xx} = \frac{1}{(L^*)^2} u_{\hat{x}\hat{x}}. \quad (13)$$

By replacing them in Eq. (6), we obtain,

$$u_{\hat{t}}(\hat{x}, \hat{t}) = u_{\hat{x}\hat{x}}(\hat{x}, \hat{t}) + \phi^2[1 - u(\hat{x}, \hat{t})] \quad (14)$$

where $\phi^2 = TL^2/4D^*$. The initial and boundary conditions are then,

$$u(0, \hat{t}) = u(1, \hat{t}) = 0, \quad \hat{t} > 0, \quad (15)$$

$$u(\hat{x}, 0) = 1, \quad 0 < \hat{x} < 1. \quad (16)$$

In the results section, we present the stationary state solution $u_E(\hat{x})$ obtained by setting $u_{\hat{t}} = 0$. Here, to derive the time dependent solution, we define,

$$v(\hat{x}, \hat{t}) = u(\hat{x}, \hat{t}) - u_E(\hat{x}). \quad (17)$$

Substituting in Eq. (14) gives,

$$v_t(\hat{x}, \hat{t}) = v_{xx}(\hat{x}, \hat{t}) - \phi^2 v(\hat{x}, \hat{t}), \quad (18)$$

and the boundary conditions are now,

$$v(0, \hat{t}) = v(1, \hat{t}) = 0, \quad \hat{t} > 0, \quad (19)$$

$$v(\hat{x}, 0) = 1 - u_E(\hat{x}), \quad 0 < \hat{x} < 1. \quad (20)$$

This set of equations is solved by separation of variables, $v(\hat{x}, \hat{t}) = X(\hat{x})T(\hat{t})$, which gives,

$$\frac{T'(\hat{t})}{T(\hat{t})} + \phi^2 = \frac{X''(\hat{x})}{X(\hat{x})}. \quad (21)$$

Imposing the initial and boundary conditions, we obtain,

$$u(\hat{x}, \hat{t}) = \frac{4}{\pi} \sum_{n=1}^{\infty} \left\{ \left[1 - \frac{\phi^2}{(2n-1)^2\pi^2 + \phi^2} \right] \frac{\sin[(2n-1)\pi\hat{x}]}{(2n-1)} e^{-[(2n-1)^2\pi^2 + \phi^2]\hat{t}} \right\} + \frac{1 + e^\phi - e^{-\phi(-1+\hat{x})} - e^{\phi\hat{x}}}{1 + e^\phi}, \quad (22)$$

which, in the limit $\hat{t} \rightarrow \infty$ gives the stationary solution in the main paper.

Dependence on Δp_0

As discussed in the main text, the properties of the tissue on each side of the substrate depend, not only on the target shape index of that side but also on the target value on the other side. Here, we explore the dependence on $\Delta p_0 = p_B - p_A$, defined as the difference in the target shape indices of both sides. For simplicity, we fix $p_B = 3.9$ and change p_A .

Figure 6 shows the time dependence of the demixing parameter for different values of Δp_0 . For all values, D_p initially decreases and saturates asymptotically. In the inset, we plot the asymptotic value of D_p as a function of Δp_0 , which reveals a non-monotonic behavior. From Eq. 11, we see that the time it takes for a cell to fully

adapt to the new side depends on both τ and Δp_0 . So, for vanishing Δp_0 , cells crossing sides swiftly adapt to the local target shape index, leading to an increase in D_p .

-
- [1] C.-M. Lo, H.-B. Wang, M. Dembo, and Y.-L. Wang, "Cell movement is guided by the rigidity of the substrate," *Biophys. J.* **79**, 144 (2000).
 - [2] L. G. Griffith and G. Naughton, "Tissue engineering—current challenges and expanding opportunities," *Science* **295**, 1009 (2002).
 - [3] A. Rabodzey, P. Alcaide, F. W. Lusinskas, and B. Ladoux, "Mechanical forces induced by the transendothelial migration of human neutrophils," *Biophys. J.* **95**, 1428 (2008).
 - [4] D. T. Tambe, C. C. Hardin, T. E. Angelini, K. Rajendran, C. Y. Park, X. Serra-Picamal, E. H. Zhou, M. H. Zaman, J. P. Butler, D. A. Weitz, J. J. Fredberg, and X. Trepat, "Collective cell guidance by cooperative inter-

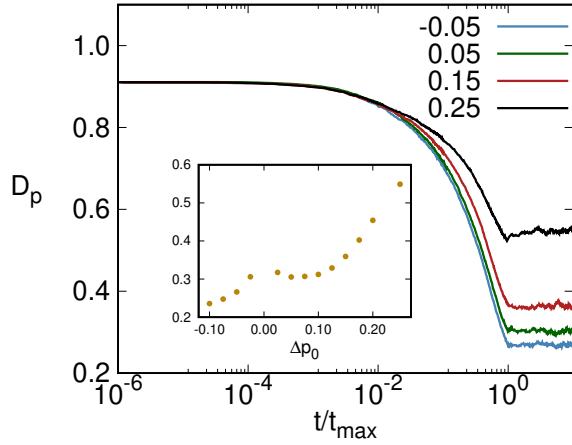


FIG. 6. Time dependence of the demixing parameter D_p , where time is rescaled by $t_{\max} = -\ln(\epsilon/\Delta p_0)$, with $N = 256$. Different curves are for different values of $\Delta p_0 = p_B - p_A$, where $p_B = 3.9$. In the inset is the asymptotic value of D_p as a function of Δp_0 . Results are averages over 10^2 samples.

- cellular forces,” *Nat. Mater.* **10**, 469 (2011).
- [5] J.-A. Park, J. H. Kim, D. Bi, J. A. Mitchel, N. T. Qazvini, K. Tantisira, C. Y. Park, M. McGill, S.-H. Kim, B. Gweon, J. Notbohm, R. S. Jr, S. Burger, S. H. Randell, A. T. Kho, D. T. Tambe, C. Hardin, S. A. Shore, E. Israel, D. A. Weitz, D. J. Tschumperlin, E. P. Henske, S. T. Weiss, M. L. Manning, J. P. Butler, J. M. Drazen, and J. J. Fredberg, “Unjamming and cell shape in the asthmatic airway epithelium,” *Nat. Mater.* **14**, 1040 (2015).
 - [6] D. E. Discher, P. Janmey, and Y. Wang, “Tissue cells feel and respond to the stiffness of their substrate,” *Science* **310**, 1139 (2005).
 - [7] W. Guo, M. T. Frey, N. A. Burnham, and Y. Wang, “Substrate rigidity regulates the formation and maintenance of tissues,” *Biophys. J.* **90**, 2213 (2006).
 - [8] S. Neuss, I. Blumenkamp, R. Stainforth, D. Boltersdorf, M. Jansen, N. Butz, A. Perez-Bouza, and R. Knüchel, “The use of a shape-memory poly(ϵ -caprolactone)dimethacrylate network as a tissue engineering scaffold,” *Biomaterials* **30**, 1697 (2009).
 - [9] M. Murrell, R. Kamm, and P. Matsudaira, “Substrate viscosity enhances correlation in epithelial sheet movement,” *Biophys. J.* **101**, 297 (2011).
 - [10] W. Song and J. F. Mano, “Interactions between cells or proteins and surfaces exhibiting extreme wettabilities,” *Soft Matter* **9**, 2985 (2013).
 - [11] R. Sunyer, V. Conte, J. Escribano, A. Elosegui-Artola, A. Labernadie, L. Valon, D. Navajas, J. M. García-Aznar, J. J. Muñoz, P. Roca-Cusachs, and X. Trepat, “Collective cell durotaxis emerges from long-range intercellular force transmission,” *Science* **353**, 1157 (2016).
 - [12] P. A. Janmey, D. A. Fletcher, and C. A. Reinhart-King, “Stiffness sensing by cells,” *Physiol. Rev.* **100**, 695 (2020).
 - [13] T. Yeung, P. C. Georges, L. A. Flanagan, B. Marg, M. Ortiz, M. Funaki, N. Zahir, W. Ming, V. Weaver, and P. A. Janmey, “Effects of substrate stiffness on cell morphology, cytoskeletal structure, and adhesion,” *Cytoskeleton* **60**, 24 (2005).
 - [14] M. Guo, A. F. Pegoraro, A. Mao, E. H. Zhou, P. R. Arany, Y. Han, D. T. Burnette, M. H. Jensen, K. E. Kasza, J. R. Moore, F. C. Mackintosh, J. J. Fredberg, D. J. Mooney, J. Lippincott-Schwartz, and D. A. Weitz, “Cell volume change through water efflux impacts cell stiffness and stem cell fate,” *PNAS* **114**, E8618 (2017).
 - [15] J. Devany, D. M. Sussman, M. L. Manning, and M. L. Gardel, “Cell division rate controls cell shape remodeling in epithelia,” *bioRxiv* (2019).
 - [16] K. A. Davis, K. A. Burke, P. T. Mather, and J. H. Henderson, “Dynamic cell behavior on shape memory polymer substrates,” *Biomaterials* **32**, 2285 (2011).
 - [17] L.-F. Tseng, P. T. Mather, and J. H. Henderson, “Shape-memory-actuated change in scaffold fiber alignment directs stem cell morphology,” *Acta Biomater.* **9**, 8790 (2013).
 - [18] H. Jeon, S. Koo, W. M. Reese, P. Loskill, C. P. Grigoropoulos, and K. E. Healy, “Directing cell migration and organization via nanocrater-patterned cell-repellent interfaces,” *Nat. Mater.* **14**, 918 (2015).
 - [19] P. Y. Mengsteab, K. Uto, A. S. T. Smith, S. Frankel, E. Fisher, Z. Nawas, J. Macadangang, M. Ebara, and D.-H. Kim, “Spatiotemporal control of cardiac anisotropy using dynamic nanotopographic cues,” *Biomaterials* **86**, 1 (2016).
 - [20] C. M. Nelson, R. P. Jean, J. L. Tan, W. F. Liu, N. J. Sniadecki, A. A. Spector, and C. S. Chen, “Emergent patterns of growth controlled by multicellular form and mechanics,” *PNAS* **102**, 11594 (2005).
 - [21] L. Richert, F. Vetrone, J. Yi, S. F. Zalzal, J. D. Wuest, F. Rosei, and A. Nanci, “Surface nanopatterning to control cell growth,” *Adv. Mater.* **20**, 1488 (2008).
 - [22] C. Horejs, “A fluid state of mind,” *Nat. Rev. Mater.* **3**, 256 (2018).
 - [23] C. Pérez-González, R. Alert, C. Blanch-Mercander, M. Gómez-González, T. Kolodziej, E. Bazellieres, J. Casademunt, and X. Trepat, “Active wetting of epithelial tissues,” *Nat. Phys.* **15**, 79 (2018).
 - [24] M. E. Brasch, G. Passucci, A. C. Gulvady, C. E. Turner, M. L. Manning, and J. H. Henderson, “Nuclear position relative to the golgi body and nuclear orientation are differentially responsive indicators of cell polarized motility,” *PLOS One* **14**, 1 (2019).
 - [25] M. S. Steinberg, “Reconstruction of tissues by dissociated cells,” *Science* **141**, 401 (1963).
 - [26] A. K. Harris, “Is cell sorting caused by differences in the work of intercellular adhesion? a critique of the steinberg hypothesis,” *J. Theor. Biol.* **61**, 267 (1976).
 - [27] G. W. Brodland, “The differential interfacial tension hypothesis (dith): A comprehensive theory for the self-rearrangement of embryonic cells and tissues,” *J. Biomech. Eng.* **124**, 188 (2002).
 - [28] R. A. Foty and M. S. Steinberg, “The differential adhesion hypothesis: a direct evaluation,” *Dev. Biol.* **278**, 255 (2005).
 - [29] J. D. Amack and M. L. Manning, “Knowing the boundaries: Extending the differential adhesion hypothesis in embryonic cell sorting,” *Science* **338**, 212 (2012).
 - [30] J.-L. Maître, H. Berthoumieux, S. F. G. Krens, G. Salbreux, F. Jülicher, E. Paluch, and C.-P. Heisenberg, “Adhesion functions in cell sorting by mechanically coupling the cortices of adhering cells,” *Science* **338**, 253 (2012).
 - [31] M. Krieg, Y. Arboleda-Estudillo, P.-H. Puech, J. Käfer,

- F. Graner, D. J. Müller, and C.-P. Heisenberg, “Tensile forces govern germ-layer organization in zebrafish,” *Nat. Cell Biol.* **10**, 429 (2008).
- [32] M. L. Manning, R. A. Foty, M. S. Steinberg, and E.-M. Schoetz, “Coaction of intercellular adhesion and cortical tension specifies tissue surface tension,” *PNAS* **107**, 12517 (2010).
- [33] D. M. Sussman, J. M. Schwarz, M. C. Marchetti, and M. L. Manning, “Soft yet sharp interfaces in a vertex model of confluent tissue,” *Phys. Rev. Lett.* **120**, 058001 (2018).
- [34] P. Sahu, D. M. Sussman, M. Rübsam, A. F. Mertz, V. Horsley, E. R. Dufresne, C. M. Niessen, M. C. Marchetti, M. L. Manning, and J. M. Schwarz, “Small-scale demixing in confluent biological tissues,” *Soft Matter* **16**, 3325 (2020).
- [35] E. Kumacheva, R. K. Golding, M. Allard, and E. H. Sargent, “Colloid crystal growth on mesoscopically patterned surfaces: Effect of confinement,” *Adv. Matter* **14**, 221 (2002).
- [36] C.-A. Fustin, G. Glasser, H. W. Spiess, and U. Jonas, “Site-selective growth of colloidal crystals with photonic properties on chemically patterned surfaces,” *Adv. Matter* **15**, 1025 (2003).
- [37] N. V. Dziomkina and G. J. Vancso, “Colloidal crystal assembly on topologically patterned templates,” *Soft Matter* **1**, 265–279 (2005).
- [38] A. Cadilhe, N. A. M. Araújo, and Vladimir Privman, “Random sequential adsorption: From continuum to lattice and pre-patterned substrates,” *J. of Phys.: Condens. Matter* **19**, 065124 (2007).
- [39] M. Ebara, “Shape-memory surfaces for cell mechanobiology,” *Sci. Technol. Adv. Mater* **16**, 014804 (2015).
- [40] D. Bi, X. Yang, M. C. Marchetti, and M. L. Manning, “Motility-driven glass and jamming transitions in biological tissues,” *Phys. Rev. X* **6**, 021011 (2016).
- [41] D. Bi, J. H. Lopez, J. M. Schwarz, and M. L. Manning, “Energy barriers and cell migration in densely packed tissues,” *Soft Matter* **10**, 1885 (2014).
- [42] D. Bi, J. H. Lopez, J. M. Schwarz, and M. L. Manning, “A density-independent rigidity transition in biological tissues,” *Nat. Phys.* **11**, 1074 (2015).
- [43] R. Farhadifar, J.-C. Röper, B. Aigouy, S. Eaton, and F. Jü, “The influence of cell mechanics, cell-cell interactions, and proliferation on epithelial packing,” *Curr. Biol.* **17**, 2095 (2007).
- [44] A. G. Fletcher, M. Osterfield, R. E. Baker, and S. Y. Shvartsman, “Vertex models of epithelial morphogenesis,” *Biophys. J.* **106**, 2291 (2014).
- [45] M. Merkel, K. Baumgarten, B. P. Tighe, and M. L. Manning, “A minimal-length approach unifies rigidity in underconstrained materials,” *PNAS* **116**, 6560 (2019).
- [46] N. A. M. Araújo, A. Cadilhe, and V. Privman, “Morphology of fine-particle monolayers deposited on nanopatterned substrates,” *Phys. Rev. E* **77**, 031603 (2008).
- [47] M. Ebara, K. Uto, N. Idota, J. Hoffman, and T. Aoyagi, “The taming of the cell: shape-memory nanopatterns direct cell orientation,” *Int. J. Nanomed* **9**, 117 (2014).
- [48] A. F. Mertz, S. Banerjee, Y. Che, G. K. German, Y. Xu, C. Hyland, M. C. Marchetti, V. Horsley, and E. R. Dufresne, “Scaling of traction forces with the size of cohesive cell colonies,” *Phys. Rev. Lett.* **108**, 198101 (2012).
- [49] X. Li, A. Das, and D. Bi, “Mechanical heterogeneity in tissues promotes rigidity and controls cellular invasion,” *Phys. Rev. Lett.* **123**, 058101 (2019).
- [50] D. M. Sussman, “cellgpu: Massively parallel simulations of dynamic vertex models,” *Comput. Phys. Commun.* **219**, 400 (2017).